24th INTERNATIONAL CONGRESS ON SOUND AND VIBRATION
23–27 July 2017, London

EFFECTS OF OSCILLATING PLATES ON AEROACOUSTIC SOUND RADIATED FROM A CASCADE OF FLAT PLATES

Y. Tanaka, H. Yokoyama, and A. Iida

Toyohashi University of Technology, Department of Mechanical Engineering, 1-1 Hibarigaoka, Tenpaku, Toyohashi-shi, Aichi 441-8580, Japan
email: tanaka@aero.me.tut.ac.jp

Intense tonal sound often radiates from the flows around a cascade of flat plates, where the acoustic resonance occurs between the plates. In order to establish methods to suppress this noise, the acoustic radiation mechanism must be clarified. The objective of this investigation is to clarify the effects of oscillation of plates on aeroacoustic fields around a cascade of flat plates, where the edges of the alternate flat plate are vibrated. Direct aeroacoustic simulations with volume penalization were conducted to understand flow and acoustic fields around the cascade of flat plates. The predicted velocity and sound pressure spectra around the cascade of flat plates are in good agreement with those of experiments. The result shows the sound pressure level decreases in the oscillation case in comparison with the non-oscillation case with increasing amplitude of oscillation at the acoustic resonant frequency. In the case of non-oscillation, the vortices shed from neighboring plates are synchronized in an anti-phase mode. However, the in-phase synchronization between the vortices shed from non-oscillated plate and oscillating plate were observed in the case of oscillating plates in some periods. This leads to the weakening of the acoustic resonance. These results also indicate that the slight oscillations of the plates could control the noise from a cascade of flat plates.
Keywords: aeroacoustics, control of aerodynamic sound

1. Introduction

Intense tonal sound often radiates from the flows around a cascade of flat plates. This configuration exists in many industrial products, such as transportation vehicles and architectures. In order to establish methods to suppress this noise, the acoustic radiation mechanism must be clarified. Parker [1] measured the sound pressure level for the flows around a cascade of flat plates and clarified that the sound pressure level becomes intense at a specific velocity and that this phenomenon is due to the coupling between the vortex shedding in the wakes and the acoustic resonance between plates. Yokoyama *et al.* [2] simulated flow and acoustic field around a cascade of flat plates. By the phase-averaged predicted flow fields around the plates, it was presented that the vortices shed from neighboring plates are synchronized in an anti-phase mode.

In the present paper, with the intention of disturbing the coupling between the vortex shedding, the edges of the alternate flat plates in the cascade of plates are arranged to be oscillated, while the other plates are static. The objective of this investigation is to clarify the effects of oscillation of plates on flow and acoustic fields around a cascade of flat plates. To do this, the direct computations of flow and acoustic fields were performed based on the compressible Navier-Stokes equations along with the volume penalization method [3-4], which is one of the various immersed boundary methods [5]. The VP method is one of the useful methods to predict flow and acoustic fields around a complex geometry and moving objects such as an oscillating plate, where the penalization term is added as external forces of the governing equations to satisfy the non-slip boundary condition inside and on the surface of the objects.

2. Computational Methodologies

2.1 Flow Configurations

The flow and acoustic fields around a cascade of five flat plates were investigated as shown in Fig. 1. Table 1 shows the computational parameters. The plate thickness, b, is 2 mm, and aspect ratio, C/b, is 15.0. The separation-to-thickness ratio, s/b, is 6.0 for the cascade of flat plates. Preliminary experiments have confirmed that acoustic resonance occurs in a half-wavelength mode along the chord length at the freestream velocity of U_0 = 44 m/s. At U_0 = 44 m/s, the Reynolds number based on the thickness and the freestream velocity is 5.8×10^3, and the freestream Mach number, $M \equiv U_0/a_0$, is 0.13. The plates are hereinafter referred to as plates A, B, C, D, and E starting from the top, as shown in Fig. 1. As shown in this figure, the x, y, and z axes are set in the flow, normal, and spanwise directions, respectively. The origin of the coordinate system is located on the spanwise middle x-y plane and at the midpoint between the upper and lower downstream edges of plate C. In the case of non-oscillation, the acoustic resonance frequency obtained from the experiment is f_{res} = 4687 Hz (St = 0.21) [2].

The parameters of oscillation of plates are shown in Table 2. The plates B and D were oscillated with a sinusoidal variation with the frequency of f_{osci}/f_{res} = 0.64 (St_{osci} = 0.14), the amplitude of A/b = 0.075 and 0.15. The ratios of the oscillation velocity to the freestream velocity, $2\pi f_{osci}A/U_0$, are 0.064 and 0.13.

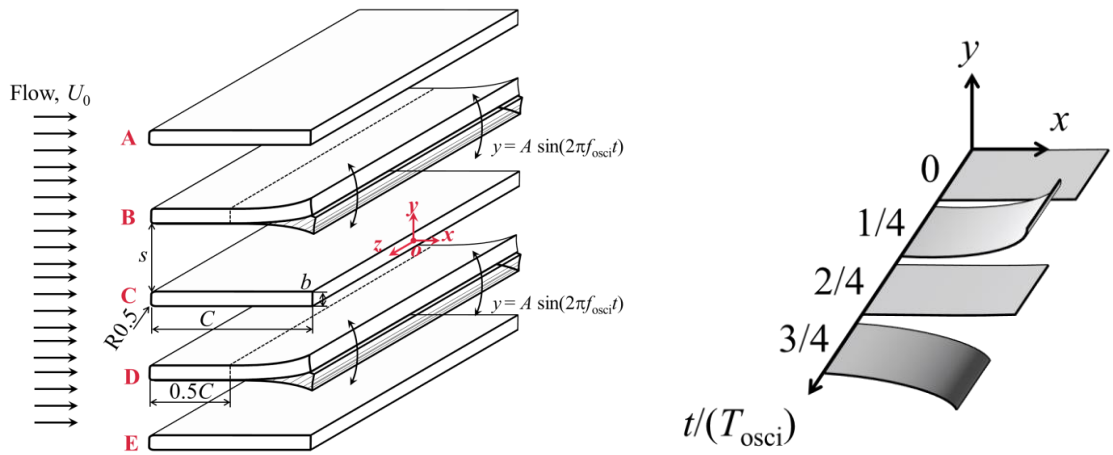

Figure 1: Configuration of flow around a cascade of flat plates.

Table 1: Computational parameters of flow around a cascade of plates

Thickness b [m]	Length C/b	Velocity U_0 [m/s]	Distance s/b	Number of plates N	Re_b
2.0×10^{-3}	15.0	44.0	6.0	5	5.8×10^3

Table 2: Parameters of oscillations of plates

Oscillation frequency f_{osci}/f_{res} [Hz]	Amplitude A/b	Oscillation velocity ratio $2\pi f_{osci}A/U_0$
0.64	0.075	0.064
	0.15	0.13

2.2 Governing Equations and Finite Difference Scheme

In order to simulate the interactions between flow and acoustic fields, the three-dimensional compressible Navier-Stokes equations were directly solved using the six-order-accurate compact finite difference scheme (the forth-order-accurate at the boundary) [6]. The time integration was performed using the third-order-accurate Runge-Kutta method. To reproduce a moving object such

as oscillating plate on rectangular grids, the VP (Volume Penalization) method was utilized. The external force, the penalization term $\boldsymbol{V}$, was added to right hand side of the governing equations of the three-dimensional compressible Navier-Stokes equations as follows:

$$\frac{\partial \boldsymbol{Q}}{\partial t}+\frac{\partial}{\partial x_k}\left(\boldsymbol{F}_k-\boldsymbol{F}_{vk}\right)=\boldsymbol{V}, \tag{1}$$

$$\boldsymbol{V}=-\left(\frac{1}{\phi}-1\right)\chi\begin{pmatrix}\partial\rho u_i/\partial x_i\\0\\0\\0\\0\end{pmatrix},\phi=0.25, \tag{2}$$

$$\chi=\begin{cases}\min\left(1,\left|d/\Delta y\right|\right) & (\text{inside object})\\ 0 & (\text{outside object})\end{cases}, \tag{3}$$

where $\boldsymbol{Q}$ is the vector of the conserved variables, $\boldsymbol{F}_{\mathrm{k}}$ is the inviscid flux vector, and $\boldsymbol{F}_{\mathrm{vk}}$ is the viscous flux vector. The coefficient ϕ is the porosity of porous medium, and determined so that the sound wave can be reflected almost completely (reflectivity: 99%). The variable of χ is the mask function, and is determined by the ratio of the distance from the surface of the object and the grid resolution, Δy, in the object, while χ is set to be zero outside the object. It has been confirmed that the flow and acoustic fields around a complex geometry can be captured by using this VP method[7].

In order to reduce the computational cost, large-eddy simulation (LES) were performed for the flow around a cascade of flat plates. No explicit SGS model was used. The turbulent energy in the GS that should be transferred to SGS eddies was dissipated by 10th-order spatial filter of Equation (4). The filter also suppressed the numerical instabilities associated with the central differencing in the compact scheme [8].

$$\alpha_{\mathrm{f}}\hat{\psi}_{i-1}+\hat{\psi}_i+\alpha_{\mathrm{f}}\hat{\psi}_{i+1}=\sum_{n=0}^{5}\frac{a_n}{2}\left(\psi_{i+n}+\psi_{i-n}\right), \tag{4}$$

where ψ is a conservative quantity, $\hat{\psi}$ is the filtered quantity. The coefficients a_n has the same values as those used by Gaitonde and Visbal [9], and the value of parameter α_{f} is 0.45.

2.3 Computational Grids

To validate the comutational schemes with the VP method, the predicted flow and acoustic fields are compared with those by the ordinary body-fitted method for a flow around the plates without oscillation. Figure 2 shows the computational grids of the body-fitted method (BF) and VP method. Also, when the VP method was used, the BF methods were also utilized for the upstream part of plates and the VP methods were combined so as to oscillate the downstream parts of the plates.

The spacings adjacent to the plate surface were $\Delta x_{\min}/b$ and $\Delta y_{\min}/b$ = 0.05. Figure 3 shows the computational domain. The spanwise extent of the computational domain was L_s/b = 15.0. In the spanwise direction, 120 grid points were used, and the spanwise grid resolution $\Delta z/b$ = 0.125 was sufficiently fine to capture the smallest active vorticies in the wake [2]. The total grids were approximately 2.5×10^7 grid points.

2.4 Boundary Conditions

Figure 3 also summarizes the boundary conditions. The inflow and outflow boundaries were artificial and so must allow vorticies and acoustic waves to pass smoothly with minimal numerical disturbances. Non-reflecting boundary conditions were used at these boundaries. Non-slip and abiabatic boundary conditions were applied at the wall of the plates. The periodic boundary conditions were used in the spanwise (z) direction.

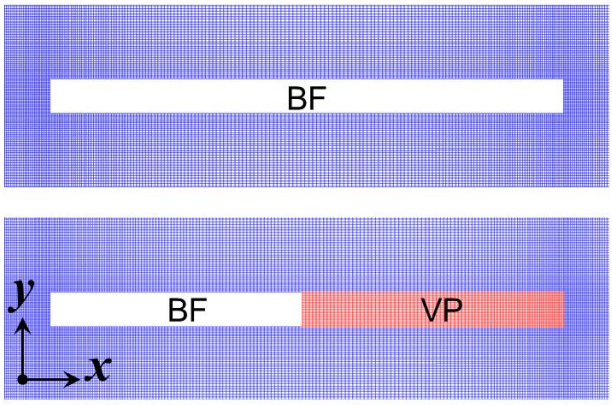

Figure 2: Computational grid.

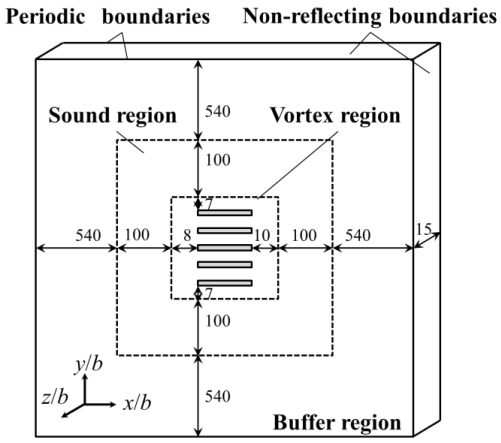

Figure 3: Computational domain and boundary condition.

2.5 Prediction of Far Acoustic Fields

In order to predict the sound pressure level at the experimental measurement point $\boldsymbol{x}_2$ (x = 0, y/b = 215), the porous FW-H method was used [10-12], as follows:

$$L_{ij} = p\delta_{ij}, \tag{6}$$

$$4\pi p'(\boldsymbol{x}_2,t) = \frac{1}{a_0}\frac{\partial}{\partial t}\int_s \left[L_{ij}(\boldsymbol{x}_1,\tau)\frac{\hat{\boldsymbol{r}}\hat{\boldsymbol{n}}}{r} \right]_{\text{ret}} dS(\boldsymbol{x}_1), \tag{7}$$

where $\boldsymbol{r} = x_2 - x_1$, $r = |\boldsymbol{r}|$, $\hat{\boldsymbol{r}} = \boldsymbol{r}/r$, and $\hat{\boldsymbol{n}}$ is the outward unit normal vector. The subscript "ret" indicates a retard time of $\tau = t - r/a_0$. The pressure, p, was sampled at the cylindrical surface at a distance from the plates of (x/b = -7.5, y = 0), r/b = 50.0. In order to estimate the sound pressure levels while taking a difference between computational and experimental spanwise extent into account, spanwise distance coherence length L_c introduced to define the equivalent length of the sound source region, as γ^2 (f, L_c) = 0.5. Sound pressure level can be estimated as follows:

$$SPL(f) = SPL_s(f) + 10\log(L/L_s) \quad (L_c(f) \le L_s), \tag{8}$$

$$SPL(f) = SPL_s(f) + 20\log(L_c(f)/L_s) + 10\log 10(L/L_c(f)) \quad (L_s < L_c(f) \le L), \tag{9}$$

$$SPL(f) = SPL_s(f) + 20\log(L/L_s) \quad (L < L_c(f)), \tag{10}$$

where the coherence, γ^2 (f, Δz), of the normal velocity fluctuations for a frequency f at two points with distance Δz in the spanwize direction along the line in the wake (x/b = 2.5, y/b = 0.5) was used.

3. Validation of Computational Methods

3.1 Flow Fields

Figure 4 shows the predicted profiles of the mean velocity and RMS values in the wake along x/b = 2.5 with that measured by a hot-wire anemometer of u_h. The duration time for the calculation of these statistical values in the computation was 0.020 s, which is shorter than that in the experiment, 30 s. In order to take this difference into consideration, the variations of the statistical values of the experimental data were estimated with the duration time shortened to the above-mentioned computational duration time and are shown as bars in Fig. 4. These results show that the profiles predicted with present computational method including the VP method is in good agreement with experimental those.

3.2 Acoustic Fields

Figure 5(a) shows the coherence of normal velocity at the fundamental frequency of St = 0.21 along the line of (x = 2.5, y/b = 0.5). It is shown that the coherence predicted by the VP method is in good agreement with that predicted by the BF method. Figure 5(b) shows the sound pressure spectrum (x = 0, y/b = 215) predicted using the methods of porous FW-H. It is shown that the level and the Strouhal number of the radiating tonal sound (St $\equiv fb/U_0$ = 0.21) predicted by both methods are in good agreement with the measured values.

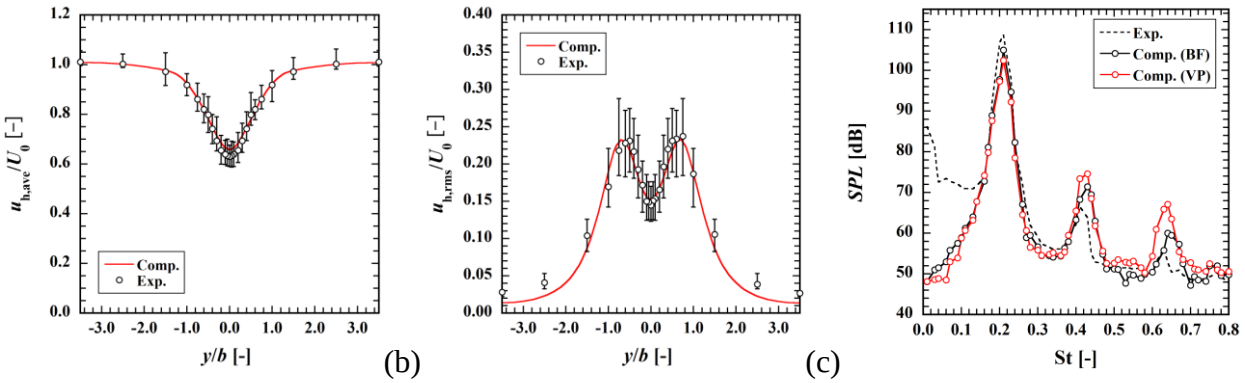

(a) (b) (c)

Figure 5: Comparison of predicted and measured velocity, u_h, profiles at x/b = 2.5 and acoustic fields. (a) Mean values. (b) RMS values. (c) Sound pressure spectra at x = 0, y/b = 215.

4. Result and Discussion

4.1 Effects of Oscillation on Sound Pressure Spectra

Figure 6 shows the sound pressure level at x/b = -7.5, y/b = 50 with and without the oscillation of plates, where the downstream edges of plates B and D are oscillated in the oscillation case. It is found that the peak frequency corresponds with the acoustic resonance frequency (St = 0.21) for non-oscillation case. By the oscillation of plates with both amplitudes of both A/b = 0.075 and 0.15, the maximum peak frequency changes to the oscillation frequency (St = 0.14). At the acoustic resonant frequency, the sound pressure level decreases in the oscillation case in comparison with the non-oscillation case with increasing amplitude of oscillation. Especially, for the oscillation case of A/b = 0.15, the sound pressure level was reduced by 10.4 dB at the acoustic resonant frequency. Consequently, the acoustic resonance can be decreased by the oscillation of the plates.

This result shows also that the aerodynamic sound changes greatly by the oscillation even if the amplitude is exceedingly smaller than the plate thickness. It is indicated that the oscillation of the objects should be taken into consideration when predicting the aerodynamic noise around the objects.

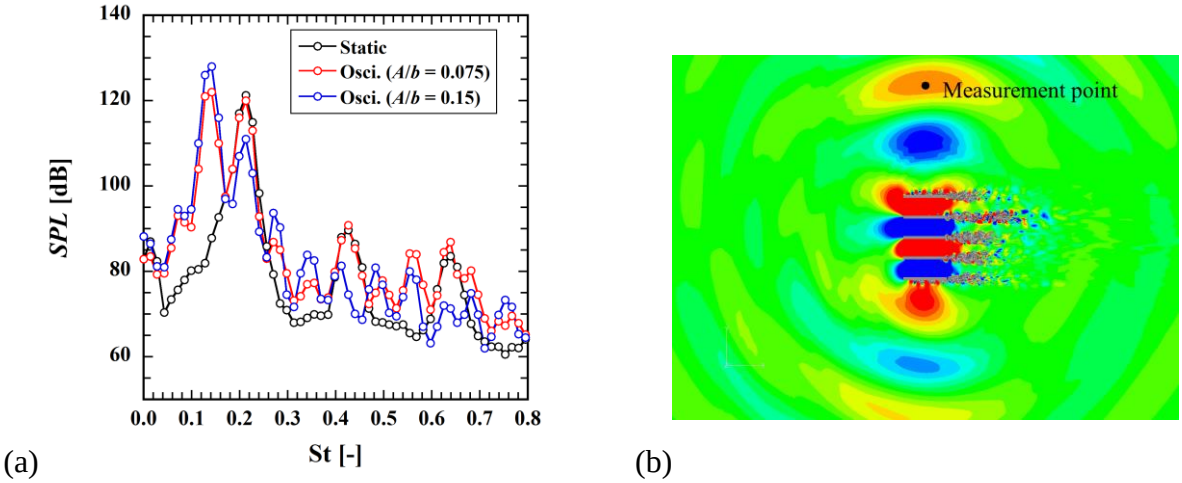

Figure 6: Effects of oscillation on sound pressure spectra (x/b = -7.5, y/b = 50).
(a) Sound pressure spectra. (b) Measurement point of sound pressure.

4.2 Power Spectra of Velocity Fluctuations

Figure 7 shows the effects of the oscillation of the plates on power spectra of u_h in the wake of plate B (x/b = 2.5, y/b = 6.5) and C(x/b = 2.5, y/b = 0.5). In the cases of static plates and plates oscillated with weak amplitude of A/b = 0.075, the maximum peak frequency of the velocity fluctuations of the flat plates B and C is the resonance frequency (St = 0.21). On the other hand, in the case of more intense oscillation with the amplitude of A/b = 0.15, the maximum peak frequency of the oscillating plate (plate B) is changed to the oscillation frequency (St = 0.14). Hence, the sound pressure level could be greatly decreased in the case of oscillation with the amplitude of A/b = 0.15 because the effects of oscillation on vortex shedding increased as the amplitude increased.

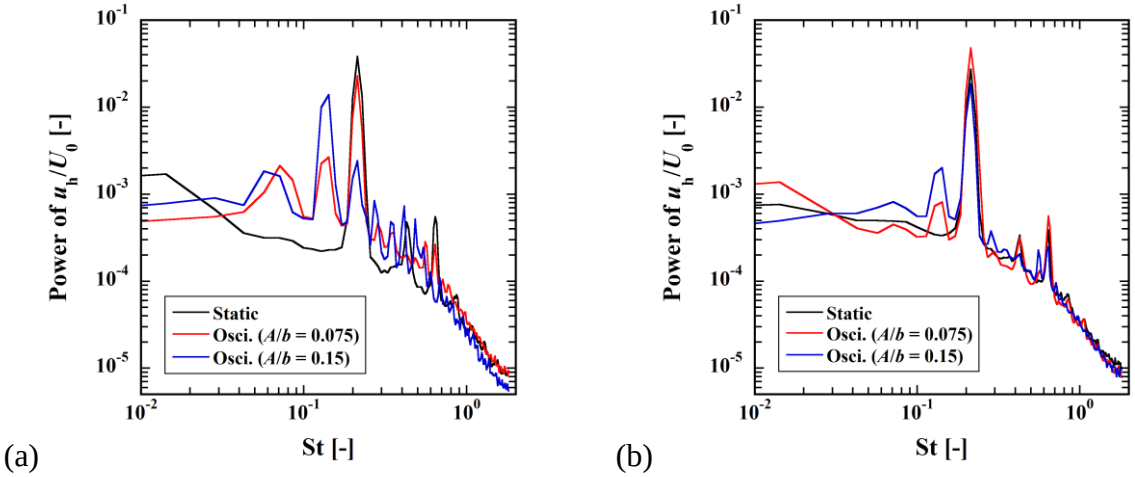

Figure 7: Effects of oscillation on power spectra of the velocity u_h.
(a) x/b = 2.5, y/b = 6.5 (in the wake of plate B). (b) x/b = 2.5, y/b = 0.5 (in the wake of plate C).

4.3 Effects of oscillation on sound radiation

Figure 8 shows the effects of oscillation on the fluctuation pressure $p'/\rho U_0$ at the streamwise midpoint of the plate (x/b = -7.5, y/b = 3.5). This shows the relationship between the oscillation displacement of plates B, D and the pressure fluctuations of the standing wave between each flat plate. The start of period, t/T_{res} = 0, is defined as a time when the vortex shedding occurs in the wake of C (x/b = 2.5, y/b = 0.5). Figure 9 shows the Iso-surfaces of the second invariant and the contours of the fluctuation pressure at the time of t/T_{res} = 0 and 0.5.

In the case of A/b = 0.075, the pressure fluctuation of the standing wave occurs with the same phase and amplitude as the case of non-oscillation until t/T_{res} = 0.5. However, the expansion be-

comes more intense by the oscillation at t/T_{res} = 1.2. This is because the plate B starts to oscillate in the upward direction and a vortex is shed from the lower edge of the plate at t/T_{res} = 0.8. As a result, the expansion waves radiating from plates B and C are reinforced.

In the case of A/b = 0.15, it is found that the difference between the pressure fluctuations without oscillation and those with the oscillation becomes more intense particulary at t/T_{res} = 1.2. Before this time (t/T_{res} = 1.0), the plate B starts to move into the downward and the vortex is shed from the upper downstream edge. As a result, a compression wave radiates and weakens the expansion wave radiating from plate C.

In the case of non-oscillation, the vortices shed from neighboring plates are synchronized in an anti-phase mode. However, the vortices shed from non-oscillated plate and oscillating plate are synchronized in an in-phase mode in some cases of oscillation. This leads to the weakening of the acoustic resonance.

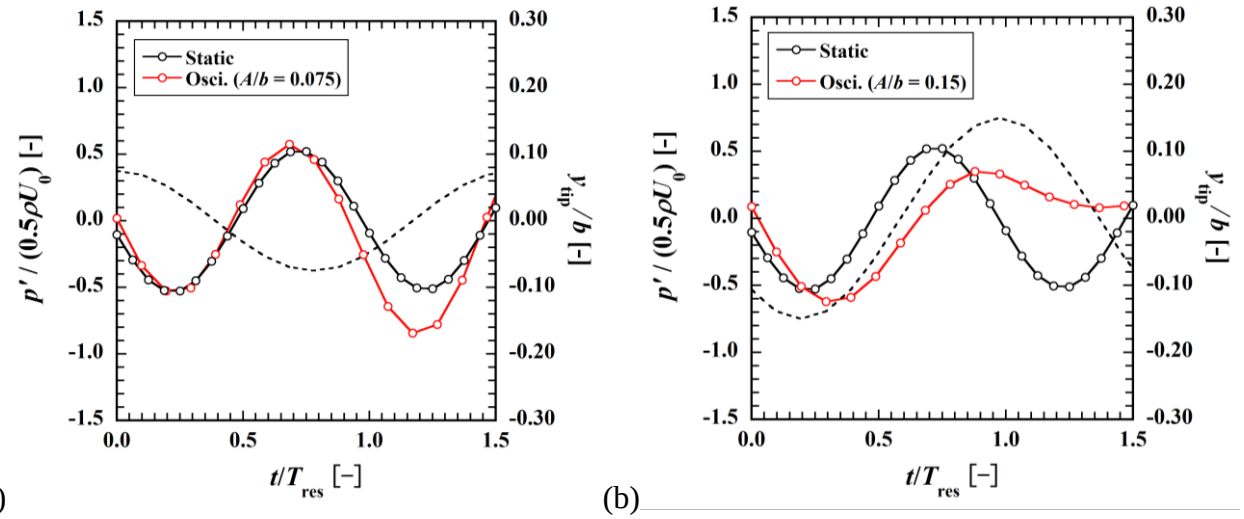

Figure 8: Effects of oscillation on fluctuation pressure $p'/\rho U_0$ between plates B and C (x/b = -7.5 and y/b = 3.5), where dotted line represents the displacement of the plates B and D. (a) A/b = 0.075. (b) A/b = 0.15.

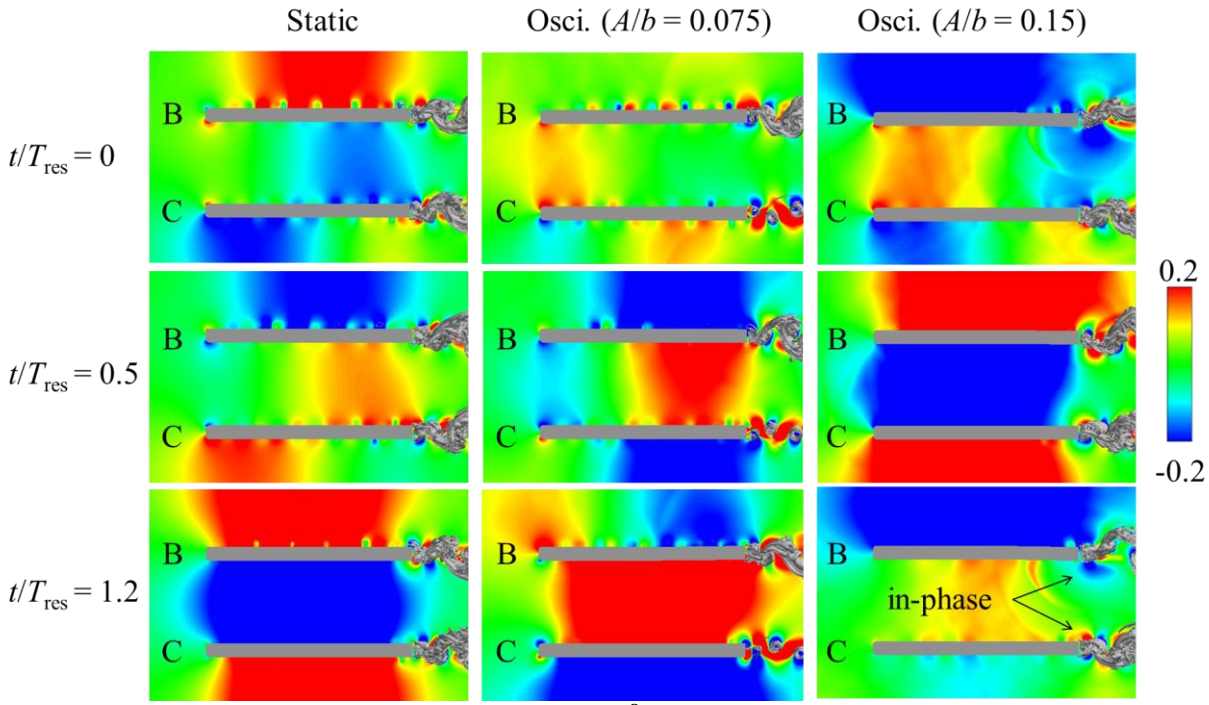

Figure 9: Iso-surfaces of the second invariant ($Q/(U_0/b)^2$ = 1.0) and the contours of the fluctuation pressure $p'/(0.5\rho U_0^2)$ focused on the plate B and C.

5. Conclusions

In order to clarify the effects of oscillation of plates on flow and acoustic fields around a cascade of flat plates, direct aeroacoustic simulations were performed.

At the acoustic resonant frequency, the sound pressure level decreases in the oscillation case in comparison with the non-oscillation case with increasing amplitude of oscillation. Especially, for the oscillation case of the ratio of the displacement to the plate thickness, A/b = 0.15, the sound pressure level was reduced by 10.4 dB at the acoustic resonant frequency. The results indicated that the acoustic resonance can be decreased by the oscillation of the plates. The oscillation of the objects should be taken into consideration when predicting the aerodynamic noise around the objects because aerodynamic sound changes greatly by the oscillation even if the amplitude is exceedingly smaller than the plate thickness.

In the case of non-oscillation, the vortices shed from neighboring plates are synchronized in an anti-phase mode. Also, the vortices shed from non-oscillated plate and oscillating plate are synchronized in an in-phase mode in some periods of oscillation. This leads to the weakening of the acoustic resonance.

6. Acknowledgement

The present study was supported by JSPS KAKENHI Grant of No. 26820044 and through the Application development for Post K computer (FLAGSHIP 2020) by the Ministry of Education, Culture, Sports, Science, and Technology of Japan (MEXT).

REFERENCES

1 Parker, R., Resonance effects in wake shedding from parallel plates: Some experimental observations, J. Sound Vib., 4(1), 67–72, (1966).

2 Yokoyama, H., Kitamiya, K., and Iida, A., Flows around a cascade of flat plates with acoustic resonance, Phys. Fluids, 25, 106104-1–22, (2013).

3 Angot, P., Bruneau, CH, and Frabrie, P., A penalization method to take into account obstacles in viscous lows, Nuner. Math., 81, 497–520, (1999).

4 Liu, Q. and Vasilyev, O. V., A Brinkman penalization method for compressible flows in comprex geometries, J. Comp. Phys., 227, 946–966, (2007).

5 Mittal, R. and Iaccarino, G., Immersed Boundary Methods, Annu. Rev. Fluid Mech., 37, 239–261, (2005) .

6 Lele, S., K., Compact finite difference schemes with spectral-like resolution, J. Comput. Phys., 103, 16–42, (1992).

7 Yokoyama, H., Miki, A., Iida, A., Direct numerical simulation of fluid-acoustic interactions in a recorder with tone holes, J. Acoust. Soc. Am., 138(2), 858–873, (2015).

8 Matsuura, K., Kato, C., Large-eddy simulation of Compressible Transitional Flows in a Low-Pressure Turbine Cascade. AIAA Journal, Vol. 45, 442–457, (2007).

9 Gaitonde, D., V. and Visbal, M., R., Pade-Type Higher-Order Boundary Filters for the Navier-Stokes Equations. AIAA Journal, Vol. 38, 2103–2112, (2000).

10 Ffowcs Williams, J., E. and Hawkings, D., L., Sound generation by turbulence and surfaces in arbitrary motion, Philos. Trans. R. Soc. London, Ser. A 264, 321, (1969).

11 Lyrintzis, A., S., Surface integral methods in computational aeroacoustics–From the (CFD) near-field to (Acoustic) far field, Int. J. Aeroacoust., 2, 95, (2003).

12 Shur, M., L., Spalart, P., R., and Strelets, M., Kh., Noise prediction for increasingly complex jets. Part 1: Methods and Tests, Int. J. Aeroacoust., 4, 213, (2005).